Systematic Comparison of the Raman Spectra of Metallic and Semiconducting SWNTs

Bo Gao,[†] Yongyi Zhang,[†] Jin Zhang,*[,†] Jing Kong,*[,‡] and Zhongfan Liu*[,†]

Centre for Nanoscale Science and Technology, Beijing National Laboratory for Molecular Sciences, Key Laboratory for the Physics and Chemistry of Nanodevices, State Key Laboratory for Structural Chemistry of Unstable and Stable Species, College of Chemistry and Molecular Engineering, Peking University, Beijing 100871, P. R. China, and Department of Electrical Engineering and Computer Science, Massachusetts Institute of Technology, Cambridge, Massachusetts 02139

Received: January 3, 2008; Revised Manuscript Received: March 11, 2008

Raman spectra of individual SWNTs were systematically investigated by comparing the behavior of 21 semiconducting and 32 metallic SWNTs. It is found that, compared to semiconducting SWNTs, the RBM of metallic ones is softened, which exhibits chirality dependence. There are significant differences in the line shape of the *G*-band between semiconducting and metallic SWNTs, which was attributed to electron–phonon coupling previously. However, we found that the differences cannot be explained only by the electron–phonon coupling via the Kohn anomaly mechanism. Curvature effect and other unknown reasons appear to also contribute to the dissimilarities. As for the *D*-band, the frequency of metallic SWNTs does not show a softening effect when compared with that of semiconducting SWNTs, which is not consistent with theoretical predictions.

Single-walled carbon nanotube (SWNT) is a unique 1-D system obtained by wrapping a graphene sheet into a seamless cylinder. Different from graphene, SWNTs can be metallic or semiconducting, depending on the wrapping direction which is specified by chiral index (n, m).[1,2] These geometry-determined differences in electronic density of states (EDOS) around the Fermi level may give rise to subtle differences in some of their physical properties, such as the Raman spectra of SWNTs.

Raman spectroscopy is an important aspect in the research of SWNTs, and also a powerful tool in characterizing SWNTs.[3,4] Generally, there are three important features in Raman spectra of SWNTs:[3] the radial breathing mode (RBM), where all carbon atoms vibrate in phase in the radial direction; the tangential *G*-band, which consists of vibrations of carbon atoms along the tube axis (LO phonon mode) or along the circumferential direction (TO phonon mode) of SWNTs; and the *D*-band, which is originated from disorder. RBM is the unique Raman active mode of SWNTs compared to other graphitic carbon systems, and is supposed to be an indication of SWNTs. Both theoretical and experimental studies have shown that the frequency of RBM is inversely proportional to the diameter of SWNTs.[5,6] *G*-Band is another widely studied Raman active mode of SWNTs, typically the TO and LO phonon modes giving rise to two separate peaks, where the higher energy peak and lower energy peak are called G^+ and G^- respectively.[7,8] *D*-Band, different from RBM and *G*-band, is due to a double resonant process.[9] Its intensity is mainly used to characterize the defects in SWNTs and other carbon materials.

In recent years there have been many investigations on the *G*-band of metallic SWNTs.[7,10,11] Experimental reports have shown that the frequency and line width of the G^- peak of metallic SWNTs are very sensitive to the position of their Fermi level[10,11] due to the electron–phonon coupling via the Kohn anomaly mechanism.[12] In contrast, investigation of the *G*-band in semiconducting SWNTs as a comparison has been rare. Comparisons for the RBM and *D*-band between individual metallic and semiconducting SWNTs and insights into the differences are also lacking. The comparisons between Raman spectra of SWNTs with and without electrons at the Fermi level may bring some interesting and unexpected observations and contribute to gain deeper insights into Raman spectra of SWNTs.

In this article, Raman spectra of individual SWNTs were systematically investigated by comparing the behavior of semiconducting and metallic SWNTs. Raman spectra of 53 individual SWNTs were analyzed. It is found that, compared to semiconducting SWNTs, the RBM of metallic ones is softened, which exhibits chirality dependence. There are significant differences in the line shape of the *G*-band between semiconducting and metallic SWNTs, which was attributed to electron–phonon coupling previously. However, we found that the differences cannot be explained only by the electron–phonon coupling via the Kohn anomaly mechanism. Curvature effect and other unknown reasons appear to also contribute to the dissimilarities. As for the *D*-band, the frequency of metallic SWNTs does not show a softening effect when compared with that of semiconducting SWNTs.

SWNTs were grown directly on Si (111) surfaces with a 200 nm thick SiO_2 layer by chemical vapor deposition (CVD).[13] Briefly, $Fe(OH)_3$ colloids hydrolyzed from $FeCl_3$ were spin-coated onto Si surfaces to act as the catalysts, and the growth was carried out at 775 °C for 5 min with a flow of ethene at 10 standard cubic centimeters per minute (sccm), and hydrogen and argon at 600 sccm, respectively. There is a significantly low density of SWNTs (shown in Figure S1, Supporting Information), so that Raman spectra from just one individual SWNT are observed. From AFM imaging, the diameters of the as-grown carbon nanotubes are mainly in the range of 1–2 nm. Raman spectral characterization was performed by using Renishaw 1000 micro-Raman spectroscopy (~1 μm spot size) with a 632.8 nm (1.959 eV) He−Ne laser with laser power of 8 mW. To ensure that SWNTs were examined parallel to laser polarization direction, lithographically etching markers were used for

* Corresponding authors. J.Z.: tel and fax, 86-10-6275-7157; e-mail, jinzhang@pku.edu.cn.
† Peking University.
‡ Massachusetts Institute of Technology.

10.1021/jp800035s CCC: $40.75
Published on Web 05/02/2008

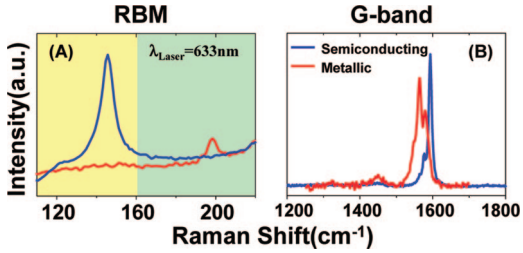

Figure 1. Typical RBM (A) and *G*-band (B) spectra of an individual (blue line) semiconducting SWNT (1# SWNT) and (red line) metallic SWNT (2# SWNT). RBM in yellow region and green region corresponds to semiconducting and metallic SWNTs respectively according to Katura plot. There is a generic difference between metallic and semiconducting SWNTs in terms of the frequency, line width of G^- and G^+ and their peak intensity ratio.

alignment.[14] All the Raman spectra were fitted to Lorentzian line shape to obtain the peak frequency, intensity and full width at half-maximum (fwhm). Chiral indices (n, m) were assigned based on the characteristic frequency, intensity and fwhm of RBM.[15]

Figure 1 shows the RBM and *G*-band spectra of two individual SWNTs. The spectra with frequency of RBM (ω_{RBM}) at 145 cm^{-1} indicate a semiconducting SWNT (1# SWNT) according to the Kataura plot.[16] The *G*-band is characteristic of semiconducting SWNTs and can be well fitted by two Lorentzian peaks. The G^+ and G^- of this semiconducting SWNT (G_S^+ and G_S^-) are located at 1593 and 1576 cm^{-1}, with narrow line width of 10 and 8 cm^{-1} respectively. And the intensity of G_S^+ is much stronger than that of G_S^-, where the peak intensity ratio of G_S^+ to G_S^- is about 6.8. The spectra with ω_{RBM} at 198 cm^{-1} correspond to a metallic SWNT (2# SWNT). The *G*-band does not show BWF line shape as reported[10,17,18] and can also be fitted by two Lorentzian peaks. Its G^+ and G^- (G_M^+ and G_M^-) are located at 1581 and 1565 cm^{-1}, with broad line width of 13 and 12 cm^{-1} respectively. In contrast to the semiconducting 1# SWNT, the intensity of G_M^- is just stronger than that of G_M^+, where the peak intensity ratio of G_M^- to G_M^+ is 1.592 (see Table S1 in Supporting Information). As will be discussed in the following, these differences are representative for the SWNTs we studied. Overall we have obtained Raman spectra from 53 individual SWNTs, 21 of which are semiconducting and 32 are metallic.

In Figure 2A, the frequency of RBM (ω_{RBM}) of 53 individual SWNTs as a function of inverse diameter ($1/d$) is plotted. The diameters are calculated from chiral indices (n, m), which are assigned based on their RBM.[15] The black squares are semiconducting SWNTs, and the red squares are metallic ones. The blue line is linearly fitted from ω_{RBM} of all 53 SWNTs. Closer examination reveals that ω_{RBM} of semiconducting SWNTs are mostly above the fitting line, whereas ω_{RBM} of metallic SWNTs are below the fitting line. This can be seen more clearly in Figures 2B and 2C, where ω_{RBM} of semiconducting and metallic SWNTs as a function of $1/d$ are plotted and fitted separately with ω_{RBM} (cm^{-1}) = A/d (nm) + B. We obtain the relation ω_{RBM}^S (cm^{-1}) = 223.4/d (nm) + 12.6 for semiconducting SWNTs resonant with E_{33}^S, and ω_{RBM}^M (cm^{-1}) = 218.3/d (nm) + 15.9 for metallic SWNTs resonant with E_{11}^M. The value A for metallic SWNTs is smaller than that for semiconducting SWNTs. First principle calculations[19] using density functional theory have predicted a similar trend: metallic SWNTs generally exhibited lower ω_{RBM} with similar diameters. Another simulation based on ensemble Monte Carlo technique showed that RBM damped the charge transport property to some extent, indicating a coupling between RBM and electrons around the Fermi level.[20] It is known that, for semiconducting SWNTs, electrons can only be excited optically between one pair of van Hove singularities (E_{11}^S, E_{22}^S, . . .); however for metallic SWNTs, besides electrons at van Hove singularities (E_{11}^M, E_{22}^M, . . .), electrons around the Fermi level can be excited to available states (E_{00}^M). These electrons, when interacting with phonons of specific energies, can lead to the modified frequencies and lifetimes for the phonons. A. Jorio[21] proposed the following functional form, ω_{RBM} (cm^{-1}) = A/d (nm) + B + (C + D $\cos^2 3\theta$)/d^2, where A described the elastic behavior of SWNTs. Hence from our result it is suggested that electron–phonon coupling lowers the elastic constants, making metallic SWNTs have smaller constant A than semiconducting ones. One more interesting phenomenon stands out in Figure 2D, where deviation of experimental ω_{RBM} of metallic SWNTs from ω_{RBM}^M ($\Delta\omega_{RBM} = \omega_{RBM} - \omega_{RBM}^M$) is plotted as a function of chiral angle θ, and from this figure we can see that metallic SWNTs close to armchair are more softened than those close to zigzag ones, indicating that the softening of RBM has some correlations with the chirality of the SWNT.

Figure 3 shows the frequency, line width and intensity of the *G*-band spectra of 53 individual SWNTs. Theoretical studies[12,22–24] have shown that for semiconducting SWNTs G_S^+ and G_S^- correspond to LO and TO phonon modes respectively; in contrast, the G_M^+ and G_M^- for metallic SWNTs should be respectively assigned to TO and LO phonon modes, since the electron–phonon coupling effect softens the LO phonon mode but not of the circumferential TO mode. Therefore we compare G_S^+ with G_M^- since they are LO phonon modes and G_S^- with G_M^+ since they are TO phonon mode. Figure 3A shows the frequency of G_M^+ and G_S^- as a function of $1/d$. The frequencies of G_M^+ center around 1584 cm^{-1}, independent of diameter (d) and chiral angle. On the other hand, the average frequency of G_S^- is smaller than that of G_M^+, and is dependent on diameter. It has been reported[7] that the frequency of G^- of individual SWNTs mode (ω_{G^-}) has a strong $1/d^2$ dependence, following the relation ω_{G^-} (cm^{-1}) = A − B/d $(nm)^2$, where A is the noncurvature frequency and B is the curvature factor. In Figure 3A, the frequency value of G_S^- can be well fitted by the equation ω_{G^-}(S) (cm^{-1}) = 1583.7 – 20.2/d $(nm)^2$, where the curvature factor is 20.2 cm^{-1}/nm^2. Note that when the diameter is close to ∞, the frequency of G_S^- approaches 1583.7 cm^{-1}, which equals the frequency of G_M^+. The observation in Figure 3A has very interesting implications. First, as there is no diameter dependence for the G_M^+ (a similar result was observed by A. Jorio[7]), it suggests that the TO phonon mode of metallic SWNTs is not affected by the curvature effects, as do the semiconducting SWNTs of similar diameter. This is surprising, and the reason for this needs further investigation. Second, if the downshift of the G_S^- relative to G_S^+ is due to curvature effect alone, the asymptote value of 1583.7 cm^{-1} should be the average frequency of the G_S^+. However, from Figure 3B one can see that the average frequency of G_S^+ is 1593 cm^{-1} (independent of diameter), which is consistent with previous experimental results,[7] but this value is higher than the results obtained by theoretical calculations.[25,26] This suggests there exist additional effect(s) for the upshift of the G_S^+ that are not considered in the theoretical calculations. In addition to the frequency of G_S^+ as a function of inverse diameter, Figure 3B also shows the frequency of G_M^-, since both correspond to the LO phonon mode. The frequency of G_S^+ is at around 1593 cm^{-1}, independent of diameter and chiral angle. But the frequency of G_M^- is much lower (~35 cm^{-1} lower on average) than that of G_S^+,

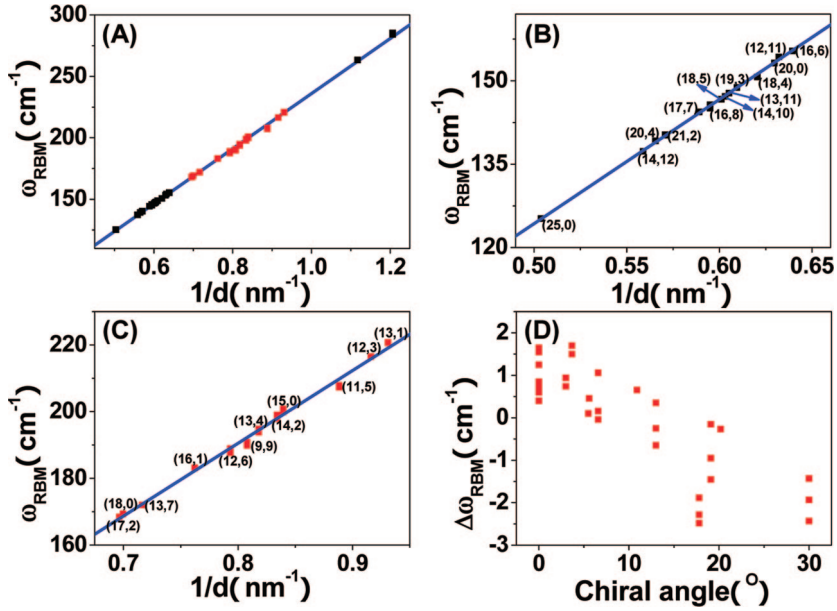

Figure 2. Frequency of RBM (ω_{RBM}) for (A) all 53 SWNTs, (B) 18 semiconducting SWNTs resonant with E_{33}^{S} and (C) 32 metallic SWNTs resonant with E_{11}^{M} as a function of inverse diameter ($1/d$). (D) Deviation of experimental ω_{RBM} of metallic SWNTs from blue lines in (C) as a function of chiral angle (θ). Black and red squares are semiconducting and metallic SWNTs respectively. Blue lines are fitting curves respectively based on (A) all 53 SWNTs, (B) 18 semiconducting SWNTs and (C) 32 metallic SWNTs. (B and C): Chiral indices are determined from RBM.

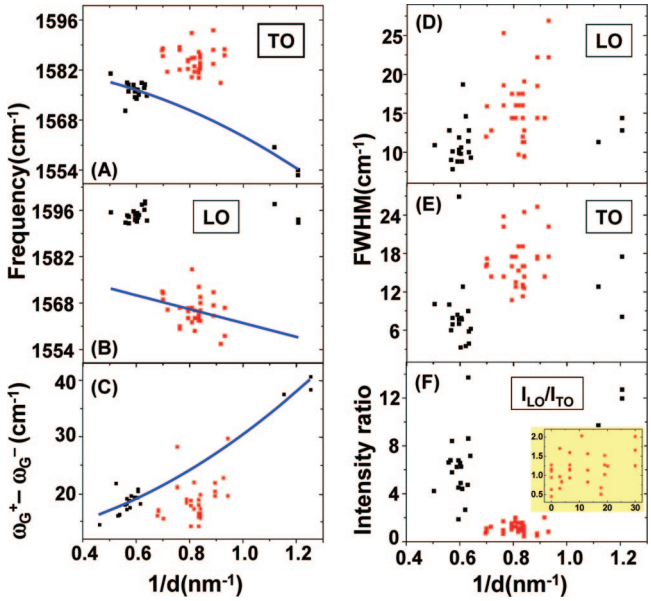

Figure 3. Lorentzian fitting results of the G-band for all 53 SWNTs as a function of inverse diameter ($1/d$): (A) frequency of the TO phonon mode-based G_S^- and G_M^+, (B) frequency of the LO phonon mode-based G_S^+ and G_M^-, (C) $\omega_{G^+} - \omega_{G^-}$, (D) line width of the LO phonon mode-based G_S^+ and G_M^-, (E) line width of the TO phonon mode-based G_S^- and G_M^+, (F) peak intensity ratio of LO to TO phonon mode. Inset of F: peak intensity ratio of LO to TO phonon mode of metallic SWNTs as a function of chiral angle. Black and red squares are semiconducting and metallic SWNTs respectively. Blue lines in A, B and C are fitting curves based on frequencies of G_S^-, G_M^- and $\omega_{G^+} - \omega_{G^-}$ of semiconducting SWNTs.

and is dependent on diameter. This is consistent with the softening due to electron–phonon coupling via the Kohn anomaly mechanism.[27] We use the relation ω_{G^-} (cm^{-1}) $= C - D/d$ (nm) to fit the frequency value of G_M^-, and get $C = 1582.9$ cm^{-1} and $D = 21.0$. With this value D it suggests that the Fermi level is away from the band crossing point, which means that the Kohn anomaly is suppressed. This is consistent with our line width observation (see discussion in the following). Figure 3C shows the $\Delta\omega_G$ ($\omega_{G^+} - \omega_{G^-}$) as a function of $1/d$. The $\Delta\omega_G$ of semiconducting SWNTs follows a relation of $1/d^2$ (the blue fitting curve). It is observed that $\Delta\omega_G$ of metallic SWNTs are below the fitting curve, which means that $\Delta\omega_G$ of metallic SWNTs are smaller than that for semiconducting ones. This observation is different from previous observations[7] where a larger frequency separation $\Delta\omega_G$ between the G^+ and G^- in metallic SWNTs was reported. Since the curvature effect is not present in the metallic SWNTs as discussed previously, the only other known factor contributing to the frequency separation $\Delta\omega_G$ is the electron–phonon coupling due to the Kohn anomaly mechanism. The relatively small $\Delta\omega_G$ is consistent with the fact that these metallic SWNTs are doped, and the Fermi level is away from the band crossing point.

It is reported[22,27] that the electron–phonon coupling effect can give rise to broadened line width of G_M^- since the LO phonon mode can decay into low-energy electron–hole excitations around the band crossing point and thus the lifetime of the phonon is reduced. As shown in Figure 3D, the average line width of G_M^- and G_S^+ (both are LO phonon mode) is 16 and 11 cm^{-1} respectively, with an average broadening of ~5 cm^{-1}, which has not been found when the LO phonon mode is Lorentzian shape.[28] In fact, theoretical calculations have predicted a line width of 60 cm^{-1} at zero doping for a (9,9) SWNT.[27] Since the metallic SWNTs in our experiments are of similar diameter, the maximum broadening should be about the same. The 5 cm^{-1} broadening in our experiments is consistent with the conclusion that the metallic SWNTs are doped and their Fermi levels are away from their band crossing point. Besides, it is noticed that the average line width of G_M^+ is broadened by 8 cm^{-1}, compared to that of G_S^- (both are TO phonon mode), which is shown in Figure 3E. Putting this observation together with the downshift of G_M^+ relative to G_S^+, it is convincing that there are some other reasons for the differences in the line width between G_M^+ and G_S^-, which needs further exploration.

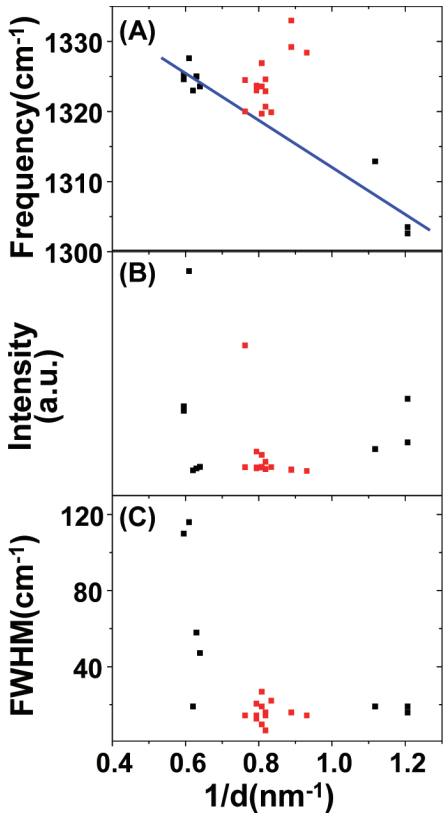

Figure 4. Lorentzian fitting results of the *D*-band for all 24 SWNTs as a function of inverse diameter (1/*d*): (A) frequency, (B) intensity, (C) line width. Black and red squares are semiconducting and metallic SWNTs respectively. Blue lines are fitting curves based on semiconducting SWNTs.

Figure 3F shows the peak intensity ratio of *G*-band as a function of 1/*d*. Here the TO phonon mode-based G_S^- and G_M^+ are taken as a reference to investigate the LO phonon mode-based G_S^+ and G_M^- by comparing the peak intensity ratio of G_M^- to G_M^+ (IR_M) with G_S^+ to G_S^- (IR_S). The IR_S for most semiconducting SWNTs are larger than 4.0, which means that the intensity of G_S^+ is much higher than that of G_S^-, whereas the IR_M for metallic SWNTs are mostly around 1.0, meaning G_M^- has almost the same intensity as G_M^+. It is noted that there is no obvious difference in the intensity of G_M^+ and G_S^-, but a remarkable decrease in the intensity of G_M^- compared to that of G_S^+ (Table S1 shown in Supporting Information). The similar intensity of G_M^+ and G_S^- indicates that the difference between the intensity of G_S^+ and G_M^- is not due to resonant conditions. Rather it may be interpreted by shorter lifetime of the LO phonon mode due to electron–phonon coupling. It is known that the intensity of resonant Raman spectra can be calculated using the equation[29]

$$I(E_{ii}) = \int \left| \frac{Mg(E)}{E_{\text{laser}} - E_{ii} - i\gamma)(E_{\text{laser}} \pm E_{\text{ph}} - E_{ii} - i\gamma} \right|^2 dE$$

where γ is the inverse lifetime of the phonon. Hence, the shorter lifetime of the LO phonon mode will bring about the remarkable decrease in the intensity of G_M^-. However, as shown in the inset of Figure 3F, the chiral angle dependence of IR_M is not observed as suspended SWNTs recently reported.[30] It may be due to the interaction between SWNTs and substrate here.

Figure 4A shows frequencies of the *D*-band (ω_D) as a function of 1/*d*. Since SWNTs directly grown by thermal CVD exhibit fewer defects, only 24 SWNTs have *D*-band and are presented here. The linear fitting shows that ω_D of semiconducting SWNTs are inversely proportional to the diameter,[31,32] with an equation ω_D (cm^{-1}) = 1345.6–33.6/*d* (nm). However, for metallic SWNTs, the frequency values are above the fitting curve, which means that the *D*-band of metallic SWNTs is hardened relative to that of semiconducting SWNTs; while in ref 32 the same equation was followed by semiconducting and metallic SWNTs.[32] Although theoretical calculations under the Kohn anomaly mechanism have predicted a stronger softening for the A_1' mode at *K* point in graphite[33,34] (which corresponds to the *D*-band phonon mode), we believe that the reason why *D*-band softening in metallic SWNTs cannot be observed is that the *D*-band Raman spectrum is double resonance in nature. As a result, the corresponding phonon that gives rise to *D*-band spectra is not exactly at the *K* point, but with a wavevector $K + k$, where *k* is proportional to the laser excitation energy. From the theoretical prediction,[21] the phonon softening is greatly reduced as the phonon wavevector moves away from the *K* point. Therefore it is reasonable that the phonon softening is not observed in metallic nanotubes. However, the hardening is unexpected too. At present we do not have a good explanation for this result. In Figures 4B and 4C, the intensity and the line width of the *D*-band as a function of 1/*d* are plotted. Since the intensity is related to both resonant conditions and defect numbers, there is not a clear difference between the semiconducting SWNTs and metallic SWNTs. But the line width of most semiconducting SWNTs is broader than that of metallic SWNTs. This is opposite to the *G*-band. It seems that the softening/hardening of the Raman active mode will be accompanied by the broadening/narrowing of the line width.

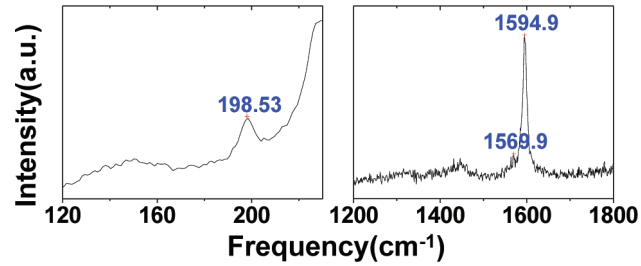

Figure 5. RBM and *G*-band spectra of an individual metallic SWNT (3# SWNT). Blue numbers are frequency.

Although most metallic SWNTs have Raman spectra different from semiconducting ones, we have also observed another four abnormal metallic SWNTs. As shown in Figure 5, one metallic SWNT (3# SWNT), with ω_{RBM} at 199 cm^{-1}, is thought to have the same chirality as 2# SWNT shown in Figure 1A. The *G*-band can be well fitted by two Lorentzian peaks. Its G^+ and G^- are located at 1596 and 1571 cm^{-1}, with line width of 13 and 19 cm^{-1} respectively. And the intensity of G^+ is much stronger than that of G^-, where the peak intensity ratio of G^+ to G^- is 20.4 (see Table S1 in Supporting Information).The *G*-band for 3# SWNT differs significantly from that for 2# SWNT, but is characteristic of *G*-band for 1# SWNT. This has been observed in ultralong SWNTs[15] and other individual SWNTs,[35] where the author[35] suggested that individual SWNTs had the same line shape, irrespective of semiconducting or metallic ones. Our experiment results contradict that argument. In most cases, *G*-bands for semiconducting and metallic SWNTs have different line shape. As for the four abnormal SWNTs, we believe that it is due to the unintentional doping during the fabrication processing or O_2 adsorption that leads to electron transfer from metallic SWNTs and weakens the electron−phonon coupling.[10] This makes it complicated to know whether a SWNT is

semiconducting or metallic from *G*-band. It is safe to determine a SWNT is metallic from *G*-band if electron–phonon coupling has a dramatic effect; however it is dangerous to determine a SWNT is semiconducting from *G*-band if electron–phonon coupling effect is not observed.

In summary, Raman spectra of individual semiconducting and metallic SWNTs were systematically compared in this article. Raman spectra of 53 individual SWNTs were analyzed. It is found that the RBM modes of the metallic SWNTs are softened compared to semiconducting SWNTs of similar diameter, which exhibits a chirality dependence. There are significant differences in the line shape of the *G*-band between semiconducting and metallic SWNTs. For the frequency, TO phonon-based G_S^- is $1/d^2$ dependent due to curvature effect, while TO phonon-based G_M^+ does not have diameter dependence, the reason for which is unknown at present. LO phonon-based G_M^- is inversely proportional to diameter due to electron–phonon coupling, while LO phonon-based G_S^+ does not have diameter dependence, which is consistent with previous reports; however the frequency of G_S^+ seems higher than theoretical calculations. The line widths of *G*-band of metallic SWNTs are broadened, where G_M^- can be attributed to electron–phonon coupling, but the reason for G_M^+ broadening is not clear. The *D*-band frequency of metallic SWNTs does not show a softening effect when compared with that of semiconducting SWNTs, which is not consistent with theoretical predictions. Finally, we observed abnormal *G*-band of another four metallic SWNTs, which was not affected by electron–phonon coupling, and it might be O_2 adsorption or other unintentional doping that eliminated its effect. Therefore it is necessary to consider their exposure to O_2 and fabrication processing in the research and application of SWNTs. Also, some interesting and unexpected observations will facilitate further modifications to theoretical calculation and contribute to gain deeper insights into Raman spectra of SWNTs.

Acknowledgment. This work was supported by NSFC (Grants 20573002, 20673004, 20725307 and 50521201) and MOST (Grants 2006CB932701, 2006CB932403, and 2007CB936203).

Supporting Information Available: Figure showing the sample and tables showing the fitting data. This material is available free of charge via the Internet at http://pubs.acs.org.

References and Notes

(1) Saito, R.; Fujita, M.; Dresselhaus, G.; Dresselhaus, M. S. *Appl. Phys. Lett.* **1992**, *60*, 2204.

(2) Wildoer, J. W. G.; Venema, L. C.; Rinzler, A. G.; Smalley, R. E.; Dekker, C. *Nature* **1998**, *391*, 59.

(3) Dresselhaus, M. S.; Eklund, P. C. *Adv. Phys.* **2000**, *49*, 705.

(4) Dresselhaus, M. S.; Dresselhaus, M. S.; Jorio, A. *J. Phys. Chem. C* **2007**, *111*, 17887.

(5) Jishi, R. A.; Venkataraman, L.; Dresselhaus, M. S.; Dresselhaus, G. *Chem. Phys. Lett.* **1993**, *209*, 77.

(6) Bachilo, S. M.; Strano, M. S.; Kittrell, C.; Hauge, R. H.; Smalley, R. E.; Weisman, R. B. *Science* **2002**, *298*, 2361.

(7) Jorio, A.; Souza, A. G.; Dresselhaus, G.; Dresselhaus, M. S.; Swan, A. K.; Unlu, M. S.; Goldberg, B. B.; Pimenta, M. A.; Hafner, J. H.; Lieber, C. M.; Saito, R. *Phys. Rev. B* **2002**, *65*, 155412.

(8) In fact, the TO and LO phonon modes each have 3 different symmetries, *A*, E_1 and E_2, so the G^+ and G^- can each contain up to three peaks. Usually only the *A* symmetry peaks show up.

(9) Thomsen, C.; Reich, S. *Phys. Rev. Lett.* **2000**, *85*, 5214.

(10) Nguyen, K. T.; Gaur, A.; Shim, M. *Phys. Rev. Lett.* **2007**, *98*, 145504.

(11) Farhat, H.; Son, H.; Samsonidze, G. G.; Reich, S.; Dresselhaus, M. S.; Kong, J. *Phys. Rev. Lett.* **2007**, *99*, 145506.

(12) Dubay, O.; Kresse, G.; Kuzmany, H. *Phys. Rev. Lett.* **2002**, *88*, 235506.

(13) Duan, X. J.; Tang, C.; Zhang, J.; Guo, W. L.; Liu, Z. F. *Nano Lett.* **2007**, *7*, 143.

(14) Shim, M.; Ozel, T.; Gaur, A.; Wang, C. J. *J. Am. Chem. Soc.* **2006**, *128*, 7522.

(15) Gao, B.; Duan, X. J.; Zhang, J.; Wu, T. J.; Son, H. B.; Kong, J.; Liu, Z. F. *Nano Lett.* **2007**, *7*, 750.

(16) Kataura, H.; Kumazawa, Y.; Maniwa, Y.; Umezu, I.; Suzuki, S.; Ohtsuka, Y.; Achiba, Y. *Synth. Met.* **1999**, *103*, 2555.

(17) Brown, S. D. M.; Jorio, A.; Corio, P.; Dresselhaus, M. S.; Dresselhaus, G.; Saito, R.; Kneipp, K. *Phys. Rev. B* **2001**, *63*, 155414.

(18) Oron-Carl, M.; Hennrich, F.; Kappes, M. M.; Lohneysen, H. V.; Krupke, R. *Nano Lett.* **2005**, *5*, 1761.

(19) Kurti, J.; Zolyomi, V.; Kertesz, M.; Sun, G. Y. *New J. Phys.* **2003**, *5*, 125.

(20) Verma, A.; Kauser, M. Z.; Ruden, P. P. *Appl. Phys. Lett.* **2005**, *87*, 123101.

(21) Jorio, A.; Fantini, C.; Pimenta, M. A.; Capaz, R. B.; Samsonidze, G. G.; Dresselhaus, G.; Dresselhaus, M. S.; Jiang, J.; Kobayashi, N.; Gruneis, A.; Saito, R. *Phys. Rev. B* **2005**, *71*, 75401.

(22) Lazzeri, M.; Piscanec, S.; Mauri, F.; Ferrari, A. C.; Robertson, J. *Phys. Rev. B* **2006**, *73*, 155426.

(23) Popov, V. N.; Lambin, P. *Phys. Rev. B* **2006**, *73*, 85407.

(24) Piscanec, S.; Lazzeri, M.; Robertson, J.; Ferrari, A. C.; Mauri, F. *Phys. Rev. B* **2007**, *75*, 35427.

(25) Sauvajol, J. L.; Anglaret, E.; Rols, S.; Alvarez, L. *Carbon* **2002**, *40*, 1697.

(26) Popov, V. N.; Lambin, P. *Physica E* **2007**, *37*, 97.

(27) Caudal, N.; Saitta, A. M.; Lazzeri, M.; Mauri, F. *Phys. Rev. B* **2007**, *75*, 115423.

(28) Jorio, A.; Fantini, C.; Dantas, M. S. S.; Pimenta, M. A.; Souza, A. G.; Samsonidze, G. G.; Brar, V. W.; Dresselhaus, G.; Dresselhaus, M. S.; Swan, A. K.; Unlu, M. S.; Goldberg, B. B.; Saito, R. *Phys. Rev. B* **2002**, *66*, 115411.

(29) Souza, A. G.; Jorio, A.; Hafner, J. H.; Lieber, C. M.; Saito, R.; Pimenta, M. A.; Dresselhaus, G.; Dresselhaus, M. S. *Phys. Rev. B* **2001**, *63*, 241404.

(30) Wu, Y.; Maultzsch, J.; Knoesel, E.; Chandra, B.; Huang, M. Y.; Sfeir, M. Y.; Brus, L. E.; Hone, J.; Heinz, T. F. *Phys. Rev. Lett.* **2007**, *99*, 27402.

(31) Pimenta, M. A.; Jorio, A.; Brown, S. D. M.; Souza, A. G.; Dresselhaus, G.; Hafner, J. H.; Lieber, C. M.; Saito, R.; Dresselhaus, M. S. *Phys. Rev. B* **2001**, *64*, 41401.

(32) Souza, A. G.; Jorio, A.; Samsonidze, G. G.; Dresselhaus, G.; Pimenta, M. A.; Dresselhaus, M. S.; Swan, A. K.; Unlu, M. S.; Goldberg, B. B.; Saito, R. *Phys. Rev. B* **2003**, *67*, 35427.

(33) Piscanec, S.; Lazzeri, M.; Mauri, F.; Ferrari, A. C.; Robertson, J. *Phys. Rev. Lett.* **2004**, *93*, 185503.

(34) Maultzsch, J.; Reich, S.; Thomsen, C.; Requardt, H.; Ordejon, P. *Phys. Rev. Lett.* **2004**, *92*, 75501.

(35) Paillet, M.; Poncharal, P.; Zahab, A.; Sauvajol, J. L.; Meyer, J. C.; Roth, S. *Phys. Rev. Lett.* **2005**, *94*, 237401.

JP800035S